Measurement 223 (2023) 113763

Contents lists available at ScienceDirect

Measurement

journal homepage: www.elsevier.com/locate/measurement

Detection and identification of cylinder misfire in small aircraft engine in different operating conditions by linear and non-linear properties of frequency components

Arkadiusz Syta [a,*], Jacek Czarnigowski [a], Piotr Jakliński [a], Norbert Marwan [b]

[a] Faculty of Mechanical Engineering, Lublin University of Technology, Nadbystrzycka 38D, Lublin, 20-618, Poland
[b] Potsdam Institute for Climate Impact Research (PIK), Potsdam, 14412, Germany

ARTICLE INFO

Keywords:
Aviation engine
Cylinder misfire
Damage detection
Machine learning
Recurrence analysis
Time series analysis

ABSTRACT

We suggest an approach for detecting and identifying ignition failure on a internal combustion engine used in aviation through the analysis of vibration time series. The research is carried out at the experimental stage, where time series of vibrations are collected from sensors installed in various parts of the facility at various rotational speeds and various operating conditions (no failure/failure of a selected piston). The time series were decomposed into periodic components centered around dominant frequencies. Data with greater dimensionality was statistically described using linear and non-linear indicators in short time windows, and labeled accordingly. Instead of examining the statistical significance of the characteristics of individual groups, machine learning classification methods were used, which allowed to distinguish the operating state of the engine (damaged/undamaged), and also to identify a specific unfired cylinder. The use of non-linear indicators allowed us to obtain 100% classification accuracy with a small number of samples.

1. Introduction

The ROTAX 912 engine is one of the most frequently used ultralight aircraft engines. It is mainly used in light aircraft with a maximum of two passengers. An important aspect of their use is to ensure flight safety. It is therefore important to monitor the operational status of the engine. Currently, only selected parameters are used, focusing mainly on the thermal condition of the engine and the efficiency of the lubrication system. There is no system allowing the diagnosis of the operation of the ignition system and the stability and repeatability of combustion based on vibrational signals [1,2]. Therefore, this work aims to develop a method of diagnostics of the operating condition based on vibrations. There are two approaches to detecting piston damage in an internal combustion engine: based on the analysis of various types of signals and based on the model. In the case of the former, we can find many examples of detecting engine misfire based on engine speed or vibroacoustic signals in the literature. Typically, the information contained in a one-dimensional signal is not sufficient to identify a misfire, and additional tools are needed to extract the characteristic features of the signal, both in the time and frequency domain. For example, adaptive filtering of the crankshaft speed [3] can extract periodic components improving misfire accuracy detection. Alternatively, Principal component analysis (PCA) and pattern recognition can be applied [4] to engine speed signals to detect and identify misfired cylinder. The combination of vibrational signals of both the crankshaft and the engine block with the use of Artificial neural networks (ANNs) [5] for best feature selection can identify the damaged piston. This type of neural network along with sliding mode observer of the crankshaft angular speed can also diagnose misfires in four-cylinder SI engine [6]. The spectral properties of vibration signals obtained by means of wavelet decomposition [7,8], as well as Fast Fourier transform (FFT) components [9], make it possible to identify damage to the pistons and clearances in the cylinders. Model systems combined with experimental data and expert systems based on fuzzy logic [10], decision trees [11], and linear trees [12] detect cylinder misfire. The accuracy of damage classification using such systems increases with the increase in the dimensionality of the data [13], as well as the wavelet decomposition [14].

This indicates that a single-channel signal may not always capture a change in the system's state (such as damage) because it contains different frequency components from different sources. It turns out that monitoring of the engine condition can be based on the decomposition of vibroacoustic signals into components with characteristic frequencies or concentrated around them. The simplest method of decomposing a signal into modes is the Empirical mode decomposition (EMD) method

* Corresponding author.
E-mail address: a.syta@pollub.pl (A. Syta).

https://doi.org/10.1016/j.measurement.2023.113763
Received 29 April 2023; Received in revised form 20 September 2023; Accepted 24 October 2023
Available online 3 November 2023

based on its envelope [15]. This algorithm was successfully used to denoise and reconstruct the signal of a properly operating small aircraft engine [16]. A extended version of the method (Multivariate empirical mode decomposition) together with the dispersion entropy [17] is able to detect fire failure in a diesel engine. Statistical characteristics of the signal components used as input to a neural network [18] are used in the diagnostics of aviation fuel pump faults. Also, the use of a Probabilistic neural network (PNN) on a dataset composed of the energy values of individual Intrinsic mode function (IMF) signals and average outlet pressure [19] allows the identification of a misfire.

Recently, the Variational Mode Decomposition (VMD) method has gained popularity, as it seems to be devoid of most of the limitations of the EMD method, such as modes mixing [20], less sensitivity to noise and sampling frequency [21–23]. This algorithm also proved useful in the process of detecting a damaged piston. The results of comparing the accuracy of classification of the EMD and VMD methods [24] indicate the advantage of the latter in the case of various damages in a diesel engine, such as valve clearance fault, fuel supply fault, and common rail pressure failure. This type of damage can also be detected using the frequency properties of the bands [25] in conjunction with a random forest model. Cross-correlation analysis between denoised and reconstructed signals with faults is also applicable here [26].

Piston misfire can also be treated as a repeatability disturbance in a non-linear system such as an internal combustion engine and non-linear time series analysis tools can be used to detect these changes [27]. Due to the possibility of applying to short and noisy time series, recurrence analysis is often used here [28,29]. The stability of the combustion process in diesel engines can be analyzed by means of recurrence indicators based on the pressure time series, which allows identifying of various properties of this process, such as determinism and laminarity [30–33]. Comparing the values of non-linear indicators (recurrence quantificators, the largest Lyapunov exponent, and the correlation dimension) confirms the non-linear character of the combustion process through sensitivity to initial conditions and system complexity [33]. Non-linear features based on recurrence indicators have already been successfully used to identify faults in rotating machines, in particular rolling bearings [34,35], as well as to predict power supply drops in power grids [36].

This research is an extension of our previous investigations on the same subject [37]. In the former research, we used linear and non-linear time series analysis to identify the misfire of the cylinder. We found that a change in the engine's operation is reflected in its dynamic response for a single measured point (fixed both engine speed and manifold air pressure). We were able to distinguish the general operational state of the engine (i.e., damaged / not damaged), but not to detect the particular piston misfired. Due to this fact, we decided that broader research is needed.

First of all, we increased the number of measurement points (compared to previous research), reducing and increasing the engine speed concerning 50% of the most common operating speed. Secondly, we increased the number of sensors by adding a new one on the plate of the engine. In addition, we examined linear and non-linear properties of both raw vibration signals and their dominant frequency components (experimental modes) in non-overlapping windows. The features generated in this way were used to train machine learning models and we analyzed the accuracy of the prediction within a certain class.

The main purpose of the work is the detection and identification of a damaged cylinder in an internal combustion engine used in aviation. In addition, the effectiveness of linear and non-linear statistics (as features) in the classification of damage in the analyzed experimental mechanical system was compared.

2. Research object

The tests were carried out on a Rotax 912 ULS engine with a modified fuel supply system. The engine tested is a four-cylinder engine in a boxer configuration, four-stroke, naturally respirated, with a dual spark ignition system. It is an engine with air cooling of the cylinders and liquid cooling of the heads and a dry sump. The engine's ignition system has two independent systems with a fixed ignition angle, with both systems operating one set of plugs each - there are two plugs in each cylinder. The motor has no flywheel and its output is connected to a 2.43:1 reduction gear equipped with overload systems and a torsional vibration damper system. The test engine was equipped with a modified intake and fuel system. A two - carburetor system was replaced by a single intake manifold with multi - point fuel injection. The fuel system is electronically controlled by a control unit from Auto & Aero Technologies and software developed by the authors of the publication, among others. Basic information about the engine is shown in Table 1. The tests were carried out at the Lublin University of Technology in a laboratory of the Department of Thermodynamics, Fluid Mechanics and Propulsion Systems (Fig. 1). The engine was installed on a bench equipped with an electric motor brake Automex 200 and connected to it using a Cardan shaft. The stand allowed thermal stabilization of the engine through heat exchanger systems in the oil and liquid cooling systems of the engine. Cylinder air cooling was provided by a blower system built into the stand. The focus of the study was on measuring engine vibrations. For this purpose, a set of six vibration sensors type PCB M353B12 was mounted using specially made brackets. The sensors were connected to amplifiers EC Electronics VibA MPPA-3000 and the amplified signal was measured by measuring instruments type National Instruments NI-9215. The sensors were placed at points, respectively (Fig. 1):

1. on the gearbox (W) in a horizontal axis perpendicular to the crankshaft rotation axis;
2. on the 1 cylinder head (1) in a piston movement axis;
3. on the 2-cylinder head (2) in a piston movement axis;
4. on the 3 cylinder head (3) in a piston movement axis;
5. on the 4 cylinder head (4) in a piston movement axis;
6. on the mounting plate (P) in a horizontal axis perpendicular to the crankshaft rotation axis.

All sensors measured vibrations on the same axis. The choice of measurement axis was based on previous research which showed that vibrations in this axis carry the most diagnostic information [37,38]. Table 2 shows the basic parameters of the analyzed signals and the accuracy of their setting (in the case of fixed parameters) and measurement (in the case of measured signals). The bench and measurement systems were selected to ensure that the measurement accuracy was an order of magnitude higher than the assumed variability under analysis. The program for recording the signals was developed in the LabView environment. Measurements were taken continuously at 30 kHz per channel.

Table 1
Specification of Rotax 912 ULS engine.

Description	Value
Type and number of cylinders	boxer 4 cylinders
Ignition type	spark ignition, doubled
Cylinder diameter	84 mm
Piston stroke	61 mm
Compression ratio	10.8 : 1
Displacement	1352 cm^3
Starting power/rotation	73.5 kW/5800 RPM
Durable/rotational power	69 kW/5500 RPM
Max. torque/rotation	128 N m/5200 RPM
Power supply	MPI system of A & A Tech
Fuel consumption - starting power	27.0 L/h
Fuel consumption - maximum constant power	25.0 L/h
Starting rotations	580 RPM
Maximum constant speed	5500 RPM
Idle speed	min. 1400 RPM

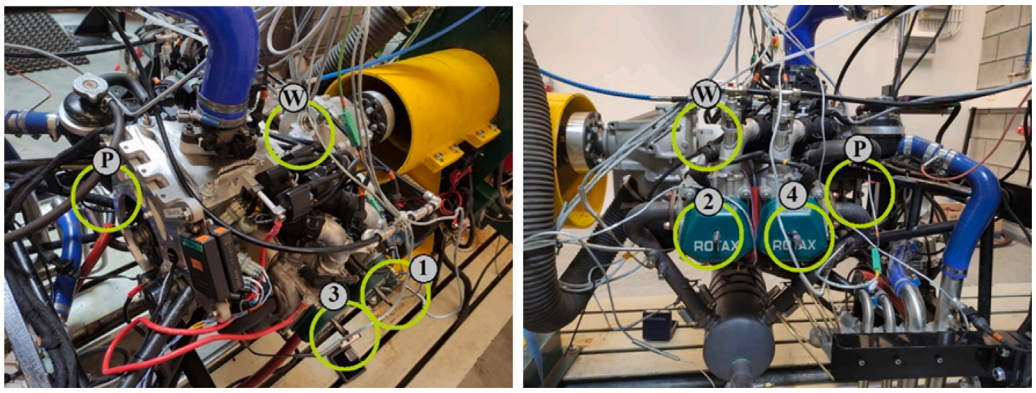

Fig. 1. Sensors mounting locations.

Table 2
Measurement accuracy and accuracy in maintaining engine operating conditions during the tests.

Signal	Sensors	Sensor accuracy	Total test error
Vibration	PCB Piezotronics PCB M353B12	Sensitivity (±10% 5 mV/g, 0.51 mV/s^2) Frequency range (±5%) 1 to 10 000 Hz Linearity ≤1%	±0.82 m/s^2
Amplifier	VibAMP PA-3000	Distortion ≤0.1%, Gain error <0.5%, Reinforcement drift <50 ppm/°C	±1.22 m/s^2
Measurement module	NI-9215	Total error 0.6% n.o., Offset 0.38% n.o.	±1%
RPM	Honeywell 1GT101DC	Total error 0.5%	±5 RPM
Engine load	Zemic H3-C3-100 kg-3B	Total error ≤0.02% n.o., Sensitivity 3 mV/V, Accuracy Class C3, Class N10	±1 N m
Ambient temperature	KTY 19-6M	Accuracy 1%	±4 °C
Ambient pressure	WIKA A-10	Non-linearity 0.25% or 0.5%, Accuracy 0.3% n.o.	±1 mbar
Ambient humidity	RHT-2H	Accuracy 3%	±1%

3. Scope of research

The study was conducted in two groups (Fig. 2):

- at a constant speed of 4000 RPM and a variable engine load expressed by manifold air pressure MAP ranging from 32 to 76 kPa (32, 42, 46, 52, 62 and 76 kPa);
- with a constant MAP load of approximately 48 kPa and engine speeds of 3000, 3500, 4000, 4500 and 5000 RPM (whereby for thermal reasons the engine load is reduced to 42 kPa at 5000 RPM).

The tests were conducted in steady-state engine operation. Five independent tests were performed for each measuring point as defined above. The first test covered the operation of the engine running correctly (marked *C*0) and the following tests the engine running with one cylinder deactivated (*C*1, *C*2, *C*3 and *C*4 respectively, where the number indicates the number of the cylinder not running). Cylinder deactivation was achieved by switching off the fuel supply in the control system. It was assumed that the constant operating parameter of the engine would be the rotational speed. This was controlled by the brake by varying the braking torque. The other operating parameters

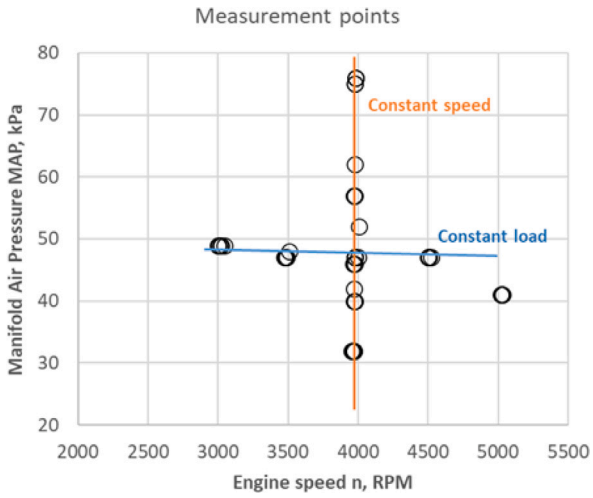

Fig. 2. Measurement points.

remained unchanged. The ignition advance angle and fuel dosage were held constant. Measurements were taken after the engine had stabilized in a given operating mode. The registration included continuous, stable engine operation for a minimum of 30 seconds. The results obtained in this way allowed a comparative analysis of the engine vibration. It should be emphasized that data directly recorded, without any preprocessing, were used for the analyses. No filtering or other signal processing was applied so that potential information on system dynamics was not lost. However, relying on such data does bring the problem of vibration sources. In the case of an aircraft, these vibrations will not only originate from the moving parts of the engine but also from the aircraft's components and the airflow. Installing vibration sensors directly on the engine reduces the strength of vibration signals from sources other than the engine itself and should not affect the results obtained. The tests were carried out with a constant engine load expressed by a constant intake manifold pressure (MAP = 48 kPa) and variable speed (Fig. 2). The base point (RPM 4000 MAP 48 kPa) was chosen based on a publication [38] showing that this is one of the most statistically occurring engine operating points. The other operating points were determined to determine the effect of engine speed (and therefore combustion frequency) on the method developed. The main objective of the research was to develop and validate methods for detecting misfires based on vibration signals. The objective was not only to indicate the occurrence of a misfire, but also to indicate which cylinder was affected. After a preliminary analysis, data from two sensors were adopted for further analysis: *W* (on the transmission) and *P* (in the engine plane). Fig. 3 shows the waveforms of the signals

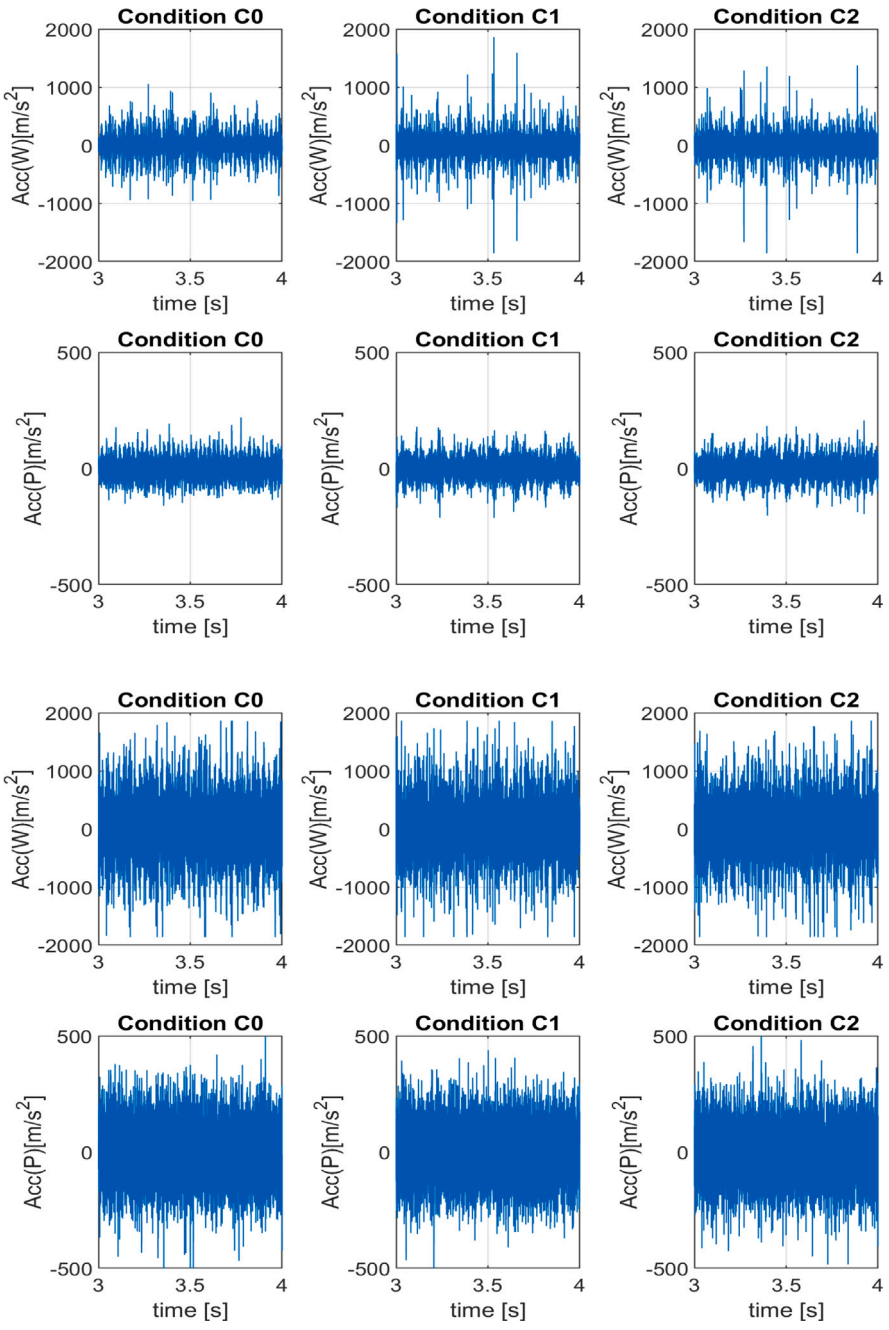

Fig. 3. Time series of raw signals for two rotational speeds, (a) 3000 RPM, (b) 5000 RPM and different operating conditions ($C0$, $C1$, $C2$).

recorded for both of these points at 3000 RPM and 5000 RPM and the various operating variants ($C0$ – engine running properly, $C1$ – cylinder 1 switch off, and $C2$ – cylinder 2 switch off). As can be observed, the level of vibration between an engine running correctly ($C0$) and one with one of the cylinders deactivated ($C1$ and $C2$) is visible for the lowest rotational speed RPM 3000 RPM, while the difference between cylinder 1 and 2 being deactivated ($C1$ and $C2$ accordingly) is not noticeable at first glance. This difference disappears at the top engine speed of 5000 RPM. Attention should also be drawn to the average vibration level recorded by the two sensors analyzed. Significantly higher levels of visible vibration were recorded for the sensor mounted on the gearbox (W) than on the cylinder plate (P). Therefore, the analysis was based not on vibration level but on frequency analysis.

4. Methods

The purpose of the analysis was to detect and identify a cylinder with a misfire through monitoring vibrations with (ideally only one) sensor. For this classification problem, we started with decomposition of the signal into a finite number of intrinsic mode functions (IMFs) that represent different frequency components using Variational Mode Decomposition (VMD) [20]. VMD is a data-driven method that does not rely on any assumptions about the underlying mathematical model of the signal. VMD works by finding the IMFs that best represent the signal using a variational principle. The algorithm iteratively adjusts the center frequency and bandwidth of each IMF until they satisfy a set of constraints that maximize the smoothness of the IMFs while minimizing their mutual interference. The final result is a set of IMFs covering the signal's frequency spectrum and representing different frequency

components. One advantage of VMD is that it can decompose non-stationary signals with time-varying frequency components, which is common in many real - world applications. VMD can also handle signals with non-linear characteristics, making it a versatile tool for signal processing. Additionally, VMD has a high level of interpretability, as each IMF corresponds to a specific frequency component of the signal. Below, a short description of the algorithm is given. Let us define the signal $x(t)$ as a sum of N amplitude and frequency - modulated signals:

$$x(t) = \sum_{n=1}^{N} v_n(t) = \sum_{n=1}^{N} A_n(t)\cos\left(\phi_n(t)\right), \tag{1}$$

where $A_n(t)$ is its amplitude and $\phi_n(t)$ is its phase. Each IMF has slowly varying and positive envelopes and a nondecreasing instantaneous frequency $\phi_n'(t)$ concentrated around the central frequency f_n. According to [20] the algorithm finds at the same time both the amplitudes of the modes v_n and their central frequencies f_n by minimizing the constrained variational problem [20]:

$$\min_{\{v_n\},\{f_n\}} \left\{ \sum_n \left\| \partial_t \left[\left(\delta(t) + \frac{j}{\pi t}\right) * v_n(t) \right] e^{-jf_n t} \right\|_2^2 \right\}, \tag{2}$$

where $\{v_n\} = \{v_1, v_2, \ldots, v_N\}$ denotes the set of all modes, $\{f_n\} = \{f_1, f_2, \ldots, f_N\}$ denotes the set of central frequencies, δ is the Dirac function, $\|\cdot\|$ is the L_2 norm and $*$ is the convolution operator. The expression $\left(\delta(t) + \frac{j}{\pi t}\right) * v_n(t)$ is the Hilbert transform of $v_n(t)$ that defines the analytical signal, and the exponential term $e^{-jf_n t}$ shifts the frequency spectrum to the baseband. The IMFs are found in the frequency domain by reconstructing DFT of the input signal $x(t)$, namely $X(f_k) = DFT(x(t))$ in terms of $V_k(f_k) = DFT(v_k(t))$. Note that the choice of the number of modes is critical. Due to the high sampling frequency (30 kHz) and the desired large number of features that describe the dynamics of the system. In our research, the number of components was $N = 15$, which means that each signal recorded at the experimental stand corresponded to 15 of time series, which were then analyzed. Then, to quantify the degree of linear correlation between the IMFs obtained from VMD and a reference signal (source vibration signal that was decomposed), the correlation coefficient was calculated:

$$\rho(x, y) = \frac{1}{N-1} \sum_{i=1}^{N} \left(\frac{x_i - \mu_x}{\sigma_x}\right)\left(\frac{y_i - \mu_y}{\sigma_y}\right), \tag{3}$$

where $x(t)$, $y(t)$ denote two signals, μ corresponds to the mean and σ corresponds to the standard deviation. A high correlation coefficient indicates that the IMF and the reference signal have a strong linear relationship, which suggests that the IMF represents a meaningful component of the original signal. On the other hand, a low correlation coefficient indicates that the IMF and the reference signal have a weak linear relationship, which suggests that the IMF may not represent a significant component of the original signal. Sample values of the correlation coefficient for individual cases are presented in Table 3:

Comparing the values of the correlation coefficient for two signal sources (W and P) and different operating conditions ($C0$, $C1$, $C2$, $C3$ and $C4$) one can notice a fairly high linear correlation for the first 4 modes. Thereafter, these values decrease to increase again for modes 9 to 12 for the data recorded by the sensor located on the gear (W). Therefore, all components were used for further analysis, due to the information about the state of the system that they may contain.

Each of the 15 modes was treated as a new signal for which linear and non-linear statistics were calculated in 0.1 s long windows. In the case of basic statistical measures, Mean, Median, Root mean square, Kurtosis and Skewness were used [39]. In the case of non-linear indicators, Determinism, Laminarity, Entropy of diagonal lines, Maximum length of the diagonal and Maximum length of the vertical line from the method of Recurrence quantitative analysis (RQA) were used [29]. The RQA is a mathematical technique used to analyze and characterize the complexity of time series data. It is a powerful tool for analyzing non-linear and chaotic systems, and has applications in a wide range of fields, including engineering and particular damage detection in combustion engines [30–33]. RQA is based on the concept of recurrence plots, which are used to visualize the recurrence of system's states over time [28,29]:

$$R_{i,j}(\varepsilon) = \Theta\left(\varepsilon - \left\|\vec{x}_i - \vec{x}_j\right\|\right), \tag{4}$$

where $\vec{x}_i$ and $\vec{x}_j$ are the states of the system, ε is the threshold value that defines the minimum distance at which two points are considered to be "recurrent", Θ is the unit step function, and $\|\cdot\|$ denotes a chosen norm (Euclidean in this case). The vector state coordinates are given numerically by solving appropriate equations of motion of the system or can be reconstructed from experimental data. Takens' embedding theorem allows us to analyze a dynamical system in space with topologically equivalent properties, such as distances between system states in time [40]. Two parameters are necessary here to be determined: a time delay and embedding dimension. The time delay should be large enough to minimize non - linear correlations between the components of the state vector. They can be determined by the first local minimum of the Mutual information function (MI) [41]. The embedding dimension should be large enough so that two points are close enough to each other in space of a given dimension, but not higher. This can be checked using the False nearest neighbor (FNN) function, which examines the distances between pairs of points in spaces of increasing dimension until the number of false neighbors drops to zero [42]. In this paper, the time delay and the embedding dimension were determined for each of the IMFs, and then the same for all cases was assumed as the median of these values, taking a time delay of 5, and the embedding dimension of 3. The values of the matrix $\mathbf{R}$ (Eq. (4)) are determined by the reconstructed state space, with 1 when two points are close enough to each other, or 0 otherwise. The visual representation of those values is the Recurrence plot (RP). Points can form vertical and horizontal lines from which certain statistics can be derived [43,44]:

- Determinism: the fraction of recurrence points that lie on diagonal lines in the recurrence plot, indicating how deterministically the system evolves.
- Entropy: a measure of the complexity or randomness of the system's dynamics.
- Laminarity: the fraction of recurrence points in vertical or horizontal lines in the recurrence plot, indicating how much the system stays in a particular state before transitioning to a different state.
- Maximal diagonal line length: providing information about the predictability and regularity of the system.
- Maximal vertical line length: providing information about the stability of and intermittency in the system.

These measures can be used to characterize different aspects of the system's dynamics and identify patterns and structures that may not be apparent from other types of analysis.

Due to the high dimensionality of the data, it was decided to use machine learning classification models instead of group statistics. The comparison of the effectiveness of linear and non-linear features was made using training and learning sets with the same number of samples and features in both cases. In the first scenario, the training set consisted of 5 linear statistics calculated for each component with the appropriate class label (75 + 1 features). The number of samples in a given class was the same (balanced data) and amounted to 80 (400 samples in total). The test set was constructed in a similar way (the same number of features - 76), but with a smaller number of samples (balanced with a total of 100). In the second scenario, the training and test data had the same number of features (76) and distribution and sample size (400 and 100, respectively), but they were generated using non-linear recurrence indicators. Both the learning and evaluation process of the models included cross-validation with 10 folds.

Table 3
Correlation coefficient between the individual IMFs and the reference signal for highest rotational speed 5000 RPM. Headers correspond to the names of the reference signals: P and W indicate the mounting position of the sensor (plate and gear, respectively), and $C0, \ldots, C4$ the number of the damaged cylinder.

	$P(C0)$	$P(C1)$	$P(C2)$	$P(C3)$	$P(C4)$	$W(C0)$	$W(C1)$	$W(C2)$	$W(C3)$	$W(C4)$
IMF_1	0.313	0.267	0.272	0.269	0.270	0.316	0.349	0.445	0.316	0.343
IMF_2	0.379	0.348	0.345	0.350	0.354	0.414	0.422	0.540	0.406	0.421
IMF_3	0.412	0.380	0.389	0.391	0.385	0.474	0.517	0.379	0.490	0.514
IMF_4	0.221	0.380	0.379	0.382	0.378	0.401	0.322	0.251	0.330	0.350
IMF_5	0.218	0.225	0.222	0.224	0.225	0.257	0.256	0.226	0.244	0.238
IMF_6	0.233	0.235	0.227	0.238	0.233	0.241	0.247	0.238	0.233	0.221
IMF_7	0.223	0.260	0.230	0.258	0.237	0.240	0.230	0.230	0.235	0.231
IMF_8	0.282	0.237	0.250	0.225	0.250	0.223	0.266	0.275	0.234	0.220
IMF_9	0.418	0.326	0.279	0.300	0.299	0.260	0.246	0.251	0.284	0.268
IMF_{10}	0.405	0.044	0.395	0.399	0.415	0.242	0.236	0.246	0.260	0.243
IMF_{11}	0.295	0.303	0.390	0.341	0.358	0.238	0.225	0.236	0.260	0.242
IMF_{12}	0.310	0.323	0.334	0.315	0.338	0.251	0.238	0.246	0.241	0.233
IMF_{13}	0.194	0.218	0.218	0.273	0.218	0.281	0.249	0.260	0.291	0.273
IMF_{14}	0.22	0.233	0.235	0.252	0.236	0.292	0.259	0.271	0.303	0.292
IMF_{15}	0.193	0.206	0.210	0.232	0.208	0.218	0.206	0.210	0.222	0.210

The entire machine learning process was carried out using the Pycaret software [45], which allows us to compare many models with each other due to different purposes. In our case, 4 models with the highest accuracy (average accuracy) value were selected: two linear models – Logistic Regression, Linear Discriminant, and two non-linear models – Random Forest and Extra Trees. It is worth noting that no optimization of hyperparameters was applied, only their default values were adopted.

Logistic regression for multiclass classification is an extension of binary logistic regression. In the classic case (binary classification), a binomial function is used to model the value of the dependent variable. For multi - label classification, a polynomial function is used with a one versus all approach in this case.

In Linear Discriminant analysis predictions are made by calculating the conditional probability that a new example belongs to a certain class and selecting the class with the highest probability. The model assumes the classes in feature space are separated by lines or hyperplanes.

Both non-linear models used in this paper are ensemble models that use multiple algorithms to improve the prediction. A Random Forest constructs multiple decision trees on different subsets of training data as it trains, which is expected to give better classification results compared to a single tree. Similarly, the Extra Trees algorithm works, but in this case a new tree is constructed with each new observation but in different subsets of features. A detailed description of the classifiers with application examples can be found in [46].

Accuracy is the most commonly used model evaluation criterion in machine learning. In the case of multi-label classification, the average accuracy (per class) is used. Both measures are derived from the confusion matrix, which is a table that counts the ratio of predicted classification (horizontal axis) to the true classification (vertical axis) [47]. In this work, both the average accuracy (for a single-valued estimation) and the error matrix (to compare the accuracy of the predictions between classes) were used to compare the performance of the models.

5. Results and discussion

To compare the selected signal processing methodology, the results of the classification of raw acceleration signals recorded by sensors located both on the transmission and the engine block are first presented (Tables 4 and 5).

Comparing the results of the classification of the training set composed of linear and non-linear features, it can be seen that they are inaccurate, but at the same time consistent, but the highest accuracy is obtained for non-linear features. The Linear Discriminant model showed the highest accuracy, and the Logistic Regression the smallest.

Table 4
Accuracy of classification results with linear features of single time series for chosen measurement points, P and W correspond to sensor notation (placement): P – plate, and W – gearbox, respectively.

Classifier	$P(3000)$	$P(3500)$	$P(4000)$	$P(4500)$	$P(5000)$
Logistic Regression	0.42	0.46	0.42	0.39	0.42
Linear Discriminant	0.42	0.47	0.47	0.44	0.41
Extra Trees	0.40	0.39	0.46	0.41	0.33
Random Forest	0.40	0.42	0.46	0.39	0.34
Classifier	$W(3000)$	$W(3500)$	$W(4000)$	$W(4500)$	$W(5000)$
Logistic Regression	0.40	0.48	0.42	0.38	0.39
Linear Discriminant	0.42	0.46	0.43	0.41	0.41
Extra Trees	0.43	0.48	0.46	0.41	0.41
Random Forest	0.41	0.46	0.45	0.39	0.41

Table 5
Accuracy of classification results with non-linear features of single time series for chosen measurement points, P and W correspond to sensor notation (placement): P – plate, and W – gearbox, respectively.

Classifier	$P(3000)$	$P(3500)$	$P(4000)$	$P(4500)$	$P(5000)$
Logistic Regression	0.33	0.18	0.31	0.34	0.32
Linear Discriminant	0.50	0.46	0.50	0.55	0.61
Extra Trees	0.45	0.41	0.47	0.53	0.57
Random Forest	0.46	0.43	0.46	0.55	0.55
Classifier	$W(3000)$	$W(3500)$	$W(4000)$	$W(4500)$	$W(5000)$
Logistic Regression	0.26	0.48	0.30	0.29	0.29
Linear Discriminant	0.43	0.46	0.46	0.47	0.48
Extra Trees	0.45	0.48	0.45	0.43	0.45
Random Forest	0.46	0.46	0.42	0.46	0.45

Seeing a lot of room for improvement, it was decided to increase the number of features, treating each of the IMFs components as a new time series. Then, the same methodology was used to determine linear and non-linear statistics for individual components. Thus, the feature space increased while maintaining the same number of observations. The results of classification using linear measures are presented in Table 6. We find a much higher accuracy of up to 0.99 when comparing the results by training the model on a linear dataset with greater dimensionality (Table 6) with the results obtained for a smaller number of features (Table 4). However, the lowest accuracy is below 0.8 ($W(3000)$ for 3 out of 4 models). Comparative results of the accuracy of identifying the damaged cylinder using non-linear features are presented in the Table 7.

The accuracy obtained for the linear set of features increases from 0.73 to 0.99 and from 4000 RPM to 5000 RPM is close to 1. It should be noted that the source of the data may be important here, especially if we compare the results for the lowest rotational speeds (3000 RPM and

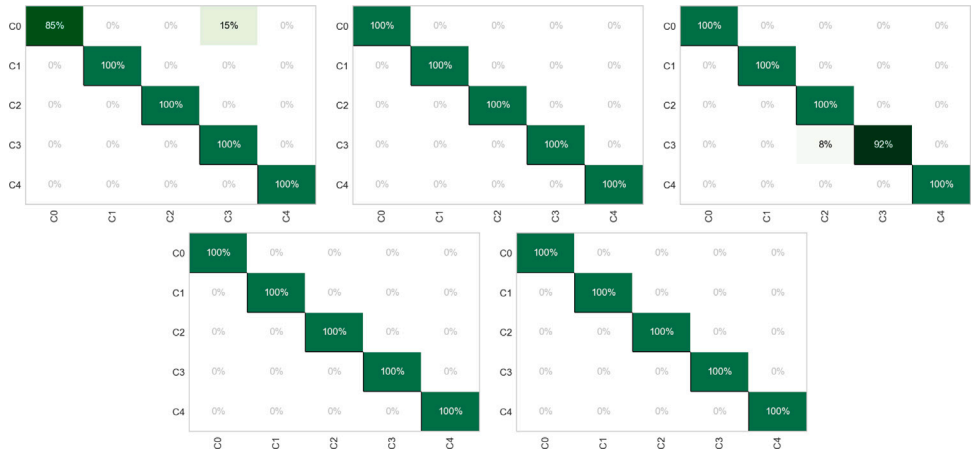

Fig. 4. Confusion matrices for Extra tree model, a sensor located at the gearbox (P), non-linear features, rotational speed increasing from the left top corner.

Table 6
Classification results with linear features of IMFs for chosen measurement points, P and W correspond to sensor notation (placement): P – plate, and W – gearbox, respectively.

Classifier	$P(3000)$	$P(3500)$	$P(4000)$	$P(4500)$	$P(5000)$
Logistic Regression	0.84	0.73	0.95	0.98	0.93
Linear Discriminant	0.85	0.79	0.97	0.99	0.96
Extra Trees	0.84	0.78	0.98	0.98	0.97
Random Forest	0.83	0.78	0.97	0.98	0.97
Classifier	$W(3000)$	$W(3500)$	$W(4000)$	$W(4500)$	$W(5000)$
Logistic Regression	0.77	0.94	0.94	0.94	0.95
Linear Discriminant	0.83	0.96	0.94	0.94	0.94
Extra Trees	0.78	0.93	0.94	0.94	0.94
Random Forest	0.78	0.92	0.93	0.95	0.92

Table 7
Classification results with non-linear features of IMFs for chosen measurement points, P and W correspond to sensor notation (placement): P – plate, and W – gearbox, respectively.

Classifier	$P(3000)$	$P(3500)$	$P(4000)$	$P(4500)$	$P(5000)$
Logistic Regression	0.99	0.98	0.96	1.00	0.98
Linear Discriminant	0.99	0.99	1.00	1.00	1.00
Extra Trees	0.99	0.99	1.00	1.00	1.00
Random Forest	0.98	0.98	0.99	1.00	1.00
Classifier	$W(3000)$	$W(3500)$	$W(4000)$	$W(4500)$	$W(5000)$
Logistic Regression	0.92	0.93	0.97	1.00	0.99
Linear Discriminant	0.99	0.99	0.99	1.00	1.00
Extra Trees	0.99	0.99	1.00	1.00	1.00
Random Forest	0.97	0.98	1.00	1.00	1.00

3500 RPM), where the discrepancy in accuracy is visible for all chosen models ($P(3000)$ versus $W(3000)$ and $P(3500)$ versus $W(3500)$).

The situation is different in the case of classification results obtained using non-linear features. While the location of the vibration sensor is important at lower speeds (3000 RPM and 3500 RPM), it is visible only for the logistic regression model. In other cases, the obtained results are comparable, close to 100% accuracy, and in most cases reaching 1.

The results of the classification on the test data for the Extra trees model (highest efficiency) are presented in Table 8.

The results of the classification accuracy of the Extra trees model on both data sets (training (Table 7) and test (Table 8)) are very similar and at the same time close to unity. This indicates that the ML model is generalizing well, and that the model has not to overfit the training data. Overfitting occurs when a model is too complex or too flexible, and it learns to fit the training data too closely, to the point that it cannot generalize well to new data. This can result in very high accuracy on the training data, but poor accuracy on the test data. Additional information about the classification results (test set) can

Table 8
Classification results of test set with non-linear features of IMFs for chosen measurement points, P and W correspond to sensor notation (placement): P – plate, and W – gearbox, respectively.

Classifier	$P(3000)$	$P(3500)$	$P(4000)$	$P(4500)$	$P(5000)$
Extra Trees	0.97	1.00	0.98	1.00	1.00
Classifier	$W(3000)$	$W(3500)$	$W(4000)$	$W(4500)$	$W(5000)$
Extra Trees	1.00	0.98	1.00	1.00	1.00

be obtained from the confusion matrix, which shows the classification results between the different classes and sensor placement: on the gearbox (W) – Fig. 4 and on the plate (P) – Fig. 5 for chosen model (extra trees in this case).

Regardless of the sensor mounting point (P or W), the classification accuracy is comparable and at a high level, but changes in different ways based on rotational speed. Namely, for sensor placed on the plate (Fig. 4) misclassifications only occur at two speeds: 3000 RPM (between $C0$ and $C3$ classes) and 4000 RPM (between $C2$ and $C3$ classes). If the sensor location is changed (Fig. 5), the misclassification occurs only at 3500 RPM (between classes $C1$ and $C3$).

6. Conclusions

In the presented work, which aimed to identify a damaged cylinder of an internal combustion engine used in the light aerospace industry, more measurements were made at various rotational speeds from 3000 RPM to 5000 RPM, as well as various mountings of sensors measuring vibrations. Identification was carried out only based on collected vibroacoustic signals and independent of the measurement point.

First, machine learning models were applied to raw experimental data to identify a damaged cylinder. For each recorded signal, five linear and non-linear statistics (as a features) were determined and machine learning classification models were used to identify the non-working cylinder. It turned out that the classification accuracy was so unsatisfactory (Tables 4 and 5) that more advanced signal processing methods had to be used to increase the dimensionality of the data using additional time series properties/features.

Then, using the VMD algorithm, the raw signals were decomposed into oscillatory components centered around characteristic frequencies. Each of the components was used as a new data source, and then the same methodology was applied (split each component into windows of the same length, calculate linear and non-linear features for each window, generate training and test sets, and then apply the same models).

It turned out that increasing the dimensionality of the data significantly improved the classification results for both linear (Table 6)

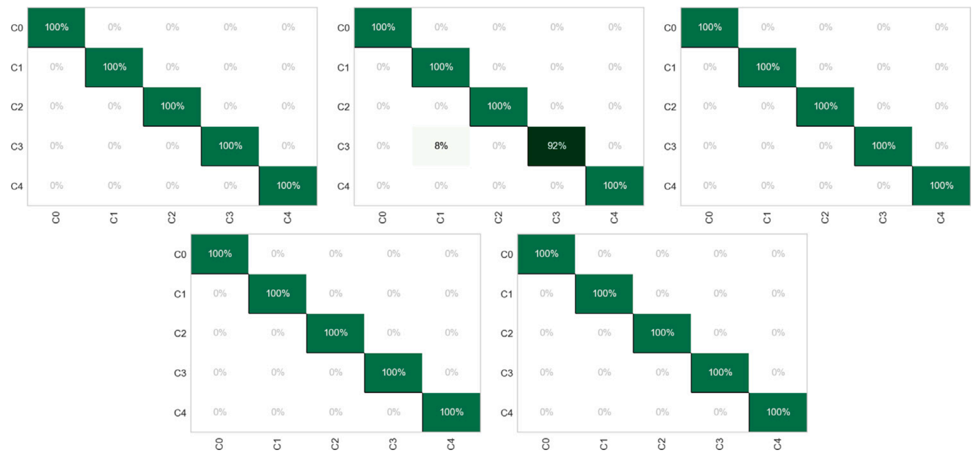

Fig. 5. Confusion matrices for Extra tree model, a sensor located at the gearbox (W), non-linear features, rotational speed increasing from the left top corner.

and non-linear (Table 7) features. The use of the latter allowed obtaining 100% accuracy in most models, for higher rotational speeds. The validation of the model with the highest accuracy (Extra trees) showed very good generalization, not deviating from the training results, which proves the lack of an overfitting effect (Table 8). The distinction between special cases, i.e., all cylinders switched on ($C0$) or one cylinder disabled ($C1$, $C2$, $C3$ or $C4$) is represented by a confusion matrix (Fig. 5) where misclassifications only occurred at lower speeds. It should be added that no optimization of the hyperparameters of the used models was applied, but only their default values, treating them as an alternative to group statistics.

It is worth noting that the performance of the model may still be limited by the specific indicators used, as well as any biases or limitations in the training data. Therefore, further exploration and validation may be necessary to fully evaluate the model's effectiveness. Also, the determination of features reflecting the non-linear properties of the dynamics of the system requires more experience than the determination of linear features.

Overall, this approach based on VMD of vibrational signals in combination with RQA has the potential to identify correctly the misfired cylinder during operation, providing a valuable tool for detecting and diagnosing cylinder misfire in small aircraft engines. The combination of both linear and non-linear features extracted from the VMD method can provide a more comprehensive analysis of the engine's behavior, leading to more accurate and reliable detection of misfire. It is worth emphasizing that only the use of non-linear measures (recurrence quantification analysis) allowed to improve the accuracy in the classification of the damaged cylinder.

CRediT authorship contribution statement

Arkadiusz Syta: Conceptualization, Investigation, Software, Writing – original draft, Writing – review & editing, Visualization. **Jacek Czarnigowski:** Supervision, Investigation, Data curation, Formal analysis, Investigation, Writing – original draft, Visualization. **Piotr Jakliński:** Data curation, Investigation, Formal analysis, Investigation, Visualization. **Norbert Marwan:** Formal analysis, Software, Writing – original draft.

Declaration of competing interest

The authors declare that they have no known competing financial interests or personal relationships that could have appeared to influence the work reported in this paper.

Data availability

Data will be made available on request.

Acknowledgment

Arkadiusz Syta would like to thank Konrad Banachewicz for an inspiring and fruitful discussion.

References

[1] S. Fábry, M. Češkovič, Aircraft gas turbine engine vibration diagnostics, MAD - Mag. Aviat. Dev. 5 (2017).
[2] J. Mohammadpour, M. Franchek, K. Grigoriadis, A survey on diagnostic methods for automotive engines, Int. J. Engine Res. 13 (2012).
[3] S. Naik, Advanced misfire detection using adaptive signal processing, Internat. J. Adapt. Control Signal Process. 2 (2004).
[4] C. Hu, A. Li, X. Zhao, Multivariate statistical analysis strategy for multiple misfire detection in internal combustion engines, Mech. Syst. Signal Process. 25 (2011).
[5] J. Chen, R. Bond Randall, Improved automated diagnosis of misfire in internal combustion engines based on simulation models, Mech. Syst. Signal Process. (2015) 64–65.
[6] T. Zheng, Y. Zhang, Y. Li, L. Shi, Real-time combustion torque estimation and dynamic misfire fault diagnosis in a gasoline engine, Mech. Syst. Signal Process. 126 (2019).
[7] Jinseok Chang, Manshik Kim, Kyoungdoug Min, Detection of misfire and knock in spark ignition engines by wavelet transform of engine block vibration signals, Meas. Sci. Technol. 13 (2002).
[8] Y. Shatnawi, M. Al-Khassaweneh, Fault diagnosis in internal combustion engines using extension neural network, IEEE Trans. Ind. Electron. 61 (2014).
[9] K. Jafarian, M. Mobin, M. Jafari-Marandi, E. Rabiei, Misfire and valve clearance faults detection in the combustion engines based on a multi-sensor vibration signal monitoring, Measurement: J. Int. Measur. Confederation 128 (2018).
[10] A. Mair, T. Thurner, Condition monitoring for reciprocating aircraft engines using fuzzy logic, in: CIMSA 2010 - IEEE International Conference on Computational Intelligence for Measurement Systems and Applications, Proceedings, 2010.
[11] S.B. Devasenapati, V. Sugumaran, K.I. Ramachandran, Misfire identification in a four-stroke four-cylinder petrol engine using decision tree, Expert Syst. Appl. 37 (2010).
[12] A. Sharma, V. Sugumaran, S. Babu Devasenapati, Misfire detection in an IC engine using vibration signal and decision tree algorithms, Measurement: J. Int. Measur. Confederation 50 (2014).
[13] Bolan Liu, Changlu Zhao, Fujun Zhang, Tao Cui, Jianyun Su, Misfire detection of a turbocharged diesel engine by using artificial neural networks, Appl. Therm. Eng. 55 (2013).
[14] C. Du, F. Jiang, K. Ding, F. Li, F. Yu, Research on feature extraction method of engine misfire fault based on signal sparse decomposition, Shock Vib. 2021 (2021).
[15] Norden E. Huang, Zheng Shen, Steven R. Long, Manli C. Wu, Hsing H. Snin, Quanan Zheng, Nai Chyuan Yen, Chi Chao Tung, Henry H. Liu, The empirical mode decomposition and the Hilbert spectrum for nonlinear and non-stationary time series analysis, Proc. R. Soc. A 454 (1998).
[16] Da Lei, Shi Sheng Zhong, Aircraft engine health signal denoising based on singular value decomposition and empirical mode decomposition methods, J. Jilin Univ. (Eng. Technol. Ed.) 43 (2013).
[17] Cheng Gu, Xin Yong Qiao, Huaying Li, Ying Jin, Misfire fault diagnosis method for diesel engine based on MEMD and dispersion entropy, Shock Vib. 2021 (5) (2021).

[18] Xiaoxuan Jiao, Bo Jing, Yifeng Huang, Wei Liang, Guangyue Xu, A fault diagnosis approach for airborne fuel pump based on EMD and probabilistic neural networks, in: Proceedings of 2016 Prognostics and System Health Management Conference, PHM-Chengdu 2016, 2017.
[19] J. Lu, F. Meng, S. Hua, L. Ding, J. Ma, Fault diagnosis for misfire and abnormal clearance in a diesel engine based on EEMD, Appl. Mech. Mater. 97 (2011).
[20] K. Dragomiretskiy, D. Zosso, Variational mode decomposition, IEEE Trans. Signal Process. 62 (2014).
[21] J. Yao, Y. Xiang, S. Qian, S. Wang, S. Wu, Noise source identification of diesel engine based on variational mode decomposition and robust independent component analysis, Appl. Acoust. 116 (2017).
[22] G. Ren, J. Jia, J. Mei, X. Jia, J. Han, Y. Wang, An improved variational mode decomposition method and its application in diesel engine fault diagnosis, J. Vibroengineering 20 (2018).
[23] Y. Liu, X. Chen, Y. Mao, Y. Chai, Y. Jiang, Fault diagnosis of sensor pulse signals based on improved energy fluctuation index and VMD, Front. Phys. 11 (2023).
[24] Xiaobo Bi, Jiansheng Lin, Daijie Tang, Fengrong Bi, Xin Li, Xiao Yang, Teng Ma, Pengfei Shen, VMD-KFCM algorithm for the fault diagnosis of diesel engine vibration signals, Energies 13 (2020).
[25] Nanyang Zhao, Zhiwei Mao, Donghai Wei, Haipeng Zhao, Jinjie Zhang, Zhinong Jiang, Fault diagnosis of diesel engine valve clearance based on variational mode decomposition and random forest, Appl. Sci. (Switzerland) 10 (2020).
[26] J. Jia, G. Ren, J. Mei, Misfire fault diagnosis of diesel engine based on VMD and XWT, Vibroeng. Procedia 24 (2019).
[27] P. Boguś, J. Merkisz, Misfire detection of locomotive diesel engine by non-linear analysis, Mech. Syst. Signal Process. 19 (2005).
[28] J.-P. Eckmann, S.O. Kamphorst, D. Ruelle, Recurrence plots of dynamical systems, Europhys. Lett. 4 (1987).
[29] N. Marwan, M. Carmenromano, M. Thiel, J. Kurths, Recurrence plots for the analysis of complex systems, Phys. Rep. 438 (2007).
[30] G. Litak, T. Kamiński, J. Czarnigowski, D. Zukowski, M. Wendeker, Cycle-to-cycle oscillations of heat release in a spark ignition engine, 42, 2007.
[31] A. Sen, R. Longwic, G. Litak, K. Górski, Analysis of cycle-to-cycle pressure oscillations in a diesel engine, Mech. Syst. Signal Process. 22 (2008).
[32] S.-L Ding, L. Yang, En-Zhe Song, Xiu-Zhen Ma, Investigations on in-cylinder pressure cycle-to-cycle variations in a diesel engine by recurrence analysis, SAE Technical Papers 2015 (2015).
[33] L. Yang, S.-L. Ding, G. Litak, En-Zhe Song, Xiu-Zhen Ma, Identification and quantification analysis of nonlinear dynamics properties of combustion instability in a diesel engine, Chaos Interdiscip. J. Nonlinear Sci. 25 (2015).
[34] H.M. Turki, Y. Chen, Z. Chaudhry, Ch Nataraj, Gear fault detection using recurrence quantification analysis and support vector machine, 11, 2018.
[35] K. Zhou, Enhanced feature extraction for machinery condition monitoring using recurrence plot and quantification measure, Int. J. Adv. Manuf. Technol. 123 (2022).
[36] A.A. Esmael, H.H. da Silva, T. Ji, R. da Silva Torres, Non-technical loss detection in power grid using information retrieval approaches: A comparative study, IEEE Access 9 (2021).
[37] A. Syta, J. Czarnigowski, P. Jakliński, Detection of cylinder misfire in an aircraft engine using linear and non-linear signal analysis, Measurement: J. Int. Measur. Confederation 174 (2021).
[38] J.A. Czarnigowski, D. Rękas, K. Ścisłowski, M. Trendak, K. Skiba, Analysis of operating parameters of the aircraft piston engine in real operating conditions, Combust. Eng. 187 (2021).
[39] R. Randall, Vibration-Based Condition Monitoring, Wiley & Sons, Ltd, 2011.
[40] F. Takens, Detecting Strange Attractors in Turbulence, Lecture Notes in Mathematics Dynamical Systems and Turbulence, Springer, Berlin/Heidelberg, 1980.
[41] A.M. Fraser, H.L. Swinney, Independent coordinates for strange attractors from mutual information, Phys. Rev. A 33 (1986).
[42] M.B. Kennel, H.D.I. Abarbanel, False neighbors and false strands: A reliable minimum embedding dimension algorithm, Phys. Rev. E 66 (2002).
[43] Ch. Webber, N. Marwan, Recurrence Quantification Analysis – Theory and Best Practices, Springer, Cham/Heidelberg, 2015.
[44] K.H. Kraemer, R.V. Donner, J. Heitzig, N. Marwan, Recurrence threshold selection for obtaining robust recurrence characteristics in different embedding dimensions, Chaos 28 (2018).
[45] Moez Ali, PyCaret: An open-source, low-code machine learning library in Python, 2020, https://www.pycaret.org.
[46] A. Gron, Hands-On Machine Learning with Scikit-Learn and TensorFlow: Concepts, Tools, and Techniques to Build Intelligent Systems, O'Reilly Media, Inc., 2017.
[47] G. Margherita, B. Enrico, V. Giorgio, Metrics for multi-class classification: An overview, 2020, ArXiv, abs/2008.05756.